

# THE MULTIPLE USES OF FLUORESCENT PROTEINS TO VISUALIZE CANCER *IN VIVO*

Robert M. Hoffman

**Abstract** | Naturally fluorescent proteins have revolutionized biology by enabling what was formerly invisible to be seen clearly. These proteins have allowed us to visualize, in real time, important aspects of cancer in living animals, including tumour cell mobility, invasion, metastasis and angiogenesis. These multicoloured proteins have allowed the colour-coding of cancer cells growing *in vivo* and enabled the distinction of host from tumour with single-cell resolution. Visualization of many aspects of cancer initiation and progression *in vivo* should be possible with fluorescent proteins.

## CHRONIC-TRANSPARENT WINDOW

A tumour grown on the inner surface of the skin that can be viewed through a permanent opening in the animal, normally through a coverslip.

## ORTHOTOPIC

Literally 'correct surface'. The implantation of a tumour (or other tissue) into its organ of origin.

## INTRAVASATION

Passage of a cell from tissue into a blood or lymph vessel.

## EXTRAVASATION

Movement of a cell out of the vasculature into interstitial spaces.

*AntiCancer Inc. and Department of Surgery, University of California, San Diego, 7917 Ostrow Street, San Diego, California 92111, USA. e-mail: all@anticancer.com*  
doi:10.1038/nrc1717

Fluorescent proteins can be used to visualize any type of cancer process, including primary tumour growth, tumour cell motility and invasion, metastatic seeding and colonization, angiogenesis, and the interaction between the tumour and its microenvironment (tumour–host interaction). Fluorescent proteins of many different colours have now been characterized and these can be used to colour-code cancer cells of a specific genotype or phenotype. For example, the behaviour of highly metastatic cancer cells labelled with green fluorescent protein (GFP) and low metastatic cancer cells labelled with red fluorescent protein (RFP) can be directly compared *in vivo*. Alternatively, the host and the tumour can be differentially labelled with fluorescent proteins — a transgenic mouse expressing GFP in all of its cells (or in specific cells such as endothelial cells) transplanted with tumour cells expressing RFP enables the interaction between the tumour cells and the host cells to be visualized in real time.

The fact that the excitation wavelengths for some fluorescent proteins are long enables real-time imaging to take place without harming the animals' tissues. Longer wavelength light causes few damaging events to proteins and DNA because of its lower energy (BOX 1). The long wavelength excitation of fluorescent proteins also reduces the extent of

photobleaching compared with dyes that have a shorter wavelength excitation. Therefore, real-time tracking of tumour growth and metastasis can be carried out in the intact animal<sup>1</sup>. For single-cell resolution, reversible acute skin-flaps as well as CHRONIC-TRANSPARENT WINDOW models can be used over many parts of the body (skin, brain, lung, liver, and so on)<sup>2–4</sup> (BOX 2). Real-time imaging with fluorescent proteins is especially important when evaluating the efficacy of therapeutics on metastasis and tumour recurrence<sup>5</sup> (see below).

## **Ex vivo imaging using fluorescent proteins**

The first use of GFP to visualize cancer cells *in vivo* was by Chishima *et al.*<sup>6</sup> They stably transfected tumour cells with GFP and transplanted these into several mouse models, including ORTHOTOPIC models that have a high metastatic capacity. They showed that in excised live tissue, with no additional preparation, metastases could be observed in any organ at the single-cell level. In addition, cells were visualized in the process of INTRAVASATION and EXTRAVASATION. The visualization of single metastatic cells in tissue is beyond the capabilities of standard histological techniques and so such *ex vivo* studies enabled, for the first time, micrometastases (including dormant cells) to be visualized in unfixed or unprocessed tissue.

## Summary

- Tumour cells can be stably transfected with fluorescent proteins.
- Tumours and metastases that express fluorescent proteins can be visualized non-invasively in intact animals.
- Transgenic mice can express a fluorescent protein in all cells or in specific cells, depending on the linkage of the fluorescent protein. These mice can be transplanted with tumours expressing different-coloured fluorescent proteins to create a dual-colour image of the tumour–host interaction.
- Tumour cells can express two or more different-coloured fluorescent proteins. For example, the nucleus can be labelled with green fluorescent protein and the cytoplasm with red fluorescent protein. This enables nuclear–cytoplasmic dynamics to be visualized *in vivo*.
- *In vivo* imaging can be at the single-cell level. For single-cell imaging on deep organs, reversible skin-flaps and chronic windows can be used. Single-cell imaging can be used to study cancer cell invasion, seeding in distant organs and dormancy.
- Fluorescent protein imaging has significant advantages over luciferase imaging, including brighter signals, substrate independence, availability in multiple colours, and simpler and cheaper equipment requirements.
- *In vivo* fluorescent imaging can be used to visualize the efficacy of candidate cancer drugs in real time in mouse models of human cancer.
- Fluorescent proteins can be used for ‘molecular imaging’ to visualize the effects of single-gene changes — for example, on cancer metastasis or drug sensitivity.
- Future uses of fluorescent proteins in human cancer diagnosis and therapy are possible — for example, in mouse models, tumours can be selectively and stably transformed *in vivo* by viral vectors. In the future such an approach might be used in humans to visualize tumour growth and response to therapy in real time.

### Intravital imaging using fluorescent proteins

Before the introduction of fluorescent proteins, *in vivo* imaging was limited to the study of cells that were transiently labelled with vital dyes. Stable fluorescent labelling, achieved using vectors that express fluorescent proteins, now allows the direct imaging of single cells *in vivo*.

Using what is termed intravital microscopy<sup>7</sup> — observation of a tumour of interest either through surgically created chronic-transparent windows or directly through the opened skin of living animals — single cancer cells have been visualized. High-resolution INTRAVITAL VIDEO MICROSCOPY of GFP-expressing tumour cells provides a powerful tool for directly observing steps in the metastatic process. Individual, non-dividing cells as well as micro- and macrometastases

can be clearly visualized and quantified. Cellular details, such as pseudopodial projections, can be clearly seen<sup>8</sup>. Farina *et al.*<sup>9</sup> observed tumour cell motility at the single-cell level, including movement in and out of blood vessels, using GFP-expressing cells. Condeelis *et al.*<sup>10</sup> have used GFP imaging to view cells in time-lapse images in a single optical section using a confocal microscope. The polarity of tumour cells, along with their response to chemotactic cytokines, has been visualized by intravital imaging<sup>9</sup>. These techniques enable a greater understanding of tumour cell migration *in vivo*.

### Imaging GFP-labelled tumour cells in blood vessels.

Tumour cell trafficking in blood vessels is an important route for metastatic spread. Visualization of this process, especially in real time, can tell us more about this pathological step. For example, following injection of tumour cells that stably express GFP into the tail vein of mice, it is possible to visualize single tumour cells in blood vessels<sup>11</sup>. Huang *et al.*, using lung carcinoma cells<sup>12</sup>, and Li *et al.*, using rodent mammary tumour cells<sup>13</sup>, observed the interaction between GFP-expressing tumour cells and the blood-vessel wall through the use of skin window chambers in rodents. They observed angiogenesis occurring very early on in tumour colony formation, when as few as 60–80 tumour cells were present. Increased vasodilation and changes in blood-vessel morphology were also observed in the surrounding tissue. When 100 cells were present, neovascularization was induced. Moore and colleagues have also visualized angiogenesis using a GFP-expressing gliosarcoma rodent cell line<sup>14</sup>.

As well as inducing angiogenesis, tumour cells also metastasize through the vasculature — this process has also been visualized. Al-Mehdi *et al.*<sup>15</sup> and Wong *et al.*<sup>16</sup> observed GFP-expressing tumour cells initiating haematogenous metastases in subpleural microvessels in intact, perfused mouse and rat lungs. Metastatic tumour cells attached to the endothelia of pulmonary precapillary arterioles and capillaries, although extravasation of the tumour cells was rare. Unexpectedly, early tumour colony formation was also observed within the blood vessels.

How do tumour cells migrate down through ever-narrowing capillaries? Work by Yamamoto and colleagues<sup>17</sup> and Yamauchi and colleagues<sup>18</sup> has addressed this by using dual-labelled cells. RFP was expressed in the cytoplasm of HT-1080 human fibrosarcoma cells, and GFP linked to histone H2B was expressed in the nucleus. The localization of fluorescent proteins depends on whether a fluorescent protein is linked to a gene encoding a protein that specifically localizes within a cellular organelle, or is located throughout the cell — an unlinked fluorescent protein would be expected to localize throughout the cell. Nuclear GFP expression enabled visualization of nuclear dynamics, whereas simultaneous cytoplasmic RFP expression enabled nuclear/cytoplasmic ratios, as well as simultaneous cell and nuclear shape changes, to be measured. By opening a skin flap on the abdomen, elongated cancer cells in capillaries in the living mice were visualized. The cells

#### CHROMOPHORES

A molecule or part of a molecule that absorbs or emits light at specific wavelengths.

#### EXTINCTION COEFFICIENT

The fractional absorbance of excitation light per unit path length of absorber.

#### QUANTUM YIELD

The fraction of excited fluorophores that emit a fluorescence photon.

### Box 1 | GFP and other fluorescent proteins as imaging agents

Green fluorescent protein (GFP) and related fluorescent proteins are a homologous protein family, having emission spectra ranging from 442 to 645 nm (REF. 74). They range in size from 25 to 30 kDa and form internal CHROMOPHORES that do not require cofactors or substrates to fluoresce. These fluorescent proteins have very high EXTINCTION COEFFICIENTS ranging from  $\epsilon = 6,500$  up to approximately  $\epsilon = 95,000$ . In addition, they have very high QUANTUM YIELDS ranging from 0.24 up to 0.8 (REF. 75). These properties make fluorescent proteins very bright. The large two-photon absorption of GFP is important for *in vivo* applications<sup>75</sup>. Another important feature is the spectral distinction between many members of the family, so a set of multicolour fluorescent proteins can be used simultaneously for multifunctional *in vivo* imaging. These properties make fluorescent proteins optimal for cellular imaging *in vivo*.

Box 2 | **How does *in vivo* imaging with fluorescent proteins work?**

The intrinsic fluorescence of these proteins is so bright that very simple equipment can be used for *in vivo* studies of tumour growth and metastasis, drug sensitivity and angiogenesis. Screening for changes in fluorescence and other macro-imaging studies requires equipment as simple as LED flashlights with appropriate excitation filters and another set of simple emission filters<sup>76</sup>.

Individual tumour cells can be detected in the live mouse using whole-body imaging with fairly simple equipment. A fluorescence light box with fibre-optic lighting at approximately 490 nm and appropriate filters, placed on top of the light box, can be used to image large tumours that can be viewed with the naked eye<sup>1</sup>. Alternatively, the light box can be linked to a camera with an appropriate filter to enable images to be displayed on a monitor and digitally stored<sup>1</sup>. To visualize smaller tumours and metastases, the animal can be put on a fluorescence dissecting microscope that incorporates a light source and filters for excitation at about 490 nm. Fluorescence emission can be observed through a 520 nm long-pass filter<sup>1</sup>. Images can be processed with standard software and the imaging procedures can be repeated as often as necessary without harming the animal. Therefore, with these techniques, real-time tracking of tumour growth and metastasis is feasible. Reversible skin-flaps can also be introduced onto different parts of the animal to look at single tumour cells or small colonies on internal organs<sup>2</sup>. The skin-flaps are rendered reversible by simple suturing. External imaging can then be done through the relatively transparent body walls of the mouse, which include the skull, by use of a fluorescence dissecting microscope. Blood vessels growing on tumours can also be observed using skin flaps because they contrast with the fluorescence of the tumours<sup>2</sup>.

Highly sophisticated equipment, including very sensitive colour charge-coupled device cameras as well as dual-photon lasers, can be used for ultra-high-resolution *in vivo* imaging of fluorescent protein expression<sup>4</sup>. Software has been developed that can automatically identify areas of fluorescence in the animals and quantify the fluorescent area and intensity.

The use of tunable filters allows the isolation of any individual spectrum in any fluorescent pixel. This technique eliminates autofluorescence as well as enabling high-resolution spectral distinction when multiple fluorescent proteins are being used. Spectral resolution enables, for example, high-resolution whole-body visualization of tumour blood vessels<sup>77</sup>.

in the capillaries elongated to fit the width of these vessels. The average length of the major axis of the cancer cells in the capillaries increased to 3.97 times their normal length. The nuclei increased their length 1.64 times in the capillaries. Non-dividing cancer cells in capillaries

over 8 µm in diameter could migrate up to 48.3 µm hr<sup>-1</sup> (FIG. 1A). These data also indicate that the minimum diameter of capillaries where cancer cells are able to migrate is approximately 8 µm. Dual-colour cells were also seen in larger vessels and occasionally some cells were seen to extravasate<sup>18</sup> (FIG. 1b). These extravasating cells can become intimately involved with blood vessels (Yamauchi, K. & R.M.H., unpublished observations) (FIG. 1c). Moreover, Chang and co-workers<sup>19</sup> used **CD31** and **CD105** to specifically identify endothelial cells and their interaction with a GFP-labelled colon carcinoma. These xenografts had mosaic vessels with focal regions in which no CD31 or CD105 immunoreactivity was detected and tumour cells appeared to contact the vessel lumen. As these and other studies have shown that tumour cells might form part of their own vasculature, these images add more weight to the argument that targeting specific endothelial markers might not have the predicted effect of significantly disrupting the tumour vasculature.

The dynamics of blood-vessel recruitment by melanoma cells was investigated by Li *et al.*<sup>20</sup> and Amoh *et al.*<sup>21</sup> They used transgenic mice expressing GFP under the control of a neural-stem-cell marker **nestin**. The nestin-regulatory-element-driven GFP (ND-GFP) has shown that nestin is expressed in hair-follicle stem cells and the blood vessel network interconnecting hair follicles in the skin. The hair follicles were shown to directly give rise to the nestin-expressing blood vessels. Following transplantation of the RFP-expressing murine melanoma cell line B16F10 into these animals, tumour angiogenesis was visualized using dual-colour fluorescence imaging. ND-GFP was expressed in the proliferating endothelial cells and nascent blood vessels in the growing tumour. Immunohistochemical staining showed that the endothelial-cell-specific antigen CD31 was expressed in ND-GFP-expressing nascent blood vessels, showing that the tumour directly recruited the nestin-expressing cells. Doxorubicin inhibited tumour angiogenesis as well as tumour growth in these mice<sup>22</sup>.

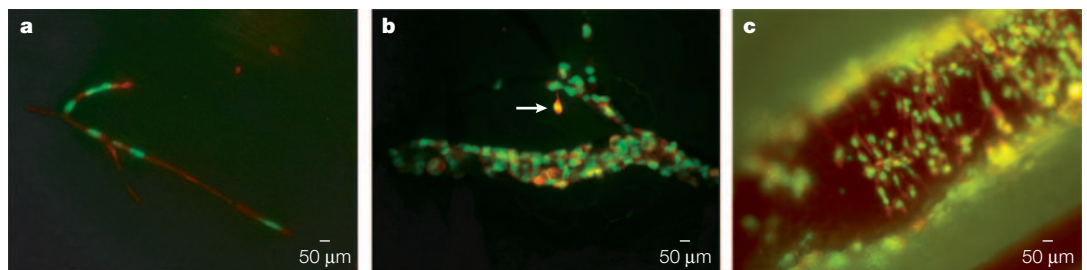


Figure 1 | **Migration of tumour cells in capillaries visualized in living animals.** **a** | The image shows HT-1080 human fibrosarcoma cells migrating in a skin capillary 14 hours after injection into the heart. Histone H2B–green fluorescent protein (GFP) is evident in the nucleus, and retrovirally expressed red fluorescent protein (RFP) is seen in the cytoplasm. Note the high degree of cell and nuclear deformation of tumour cells. Image courtesy of K. Yamauchi, N. Yamamoto, P. Jiang, and R.M.H. **b** | This image shows an HT-1080 human fibrosarcoma cell, expressing GFP in the nucleus and RFP in the cytoplasm, extravasating from a blood vessel in the skin (indicated by the arrow). Note that the blood vessel contains numerous tumour cells. The extravasating cell was visualized 2 hours after cell injection of the labelled tumour cells into the heart. Image courtesy of K. Yamauchi, N. Yamamoto, P. Jiang and R.M.H. **c** | This image shows extravasated Lewis lung carcinoma cells growing within a blood vessel. These cells were labelled in the nucleus with histone H2B–GFP and in the cytoplasm with a retrovirally-expressed RFP. The dual-colour cells were injected into the epigastric cranialis vein and the image from a live mouse with a skin flap was taken 120 hours post-injection. Image courtesy of K. Yamauchi and R.M.H.

INTRAVITAL VIDEO  
MICROSCOPY  
*In vivo* microscopy of a live animal with images acquired in real time.

Brown *et al.*<sup>4</sup> showed that MULTIPHOTON LASER-SCANNING MICROSCOPY (MPLSM)<sup>23</sup> could provide high-resolution three-dimensional images of angiogenesis-associated gene expression and that this technique could be used to investigate deeper regions of GFP-expressing tumours in dorsal skin-fold chambers. MPLSM offers significant advantages over other visualization techniques, such as improved signal/background ratios and longer sample lifetimes, as well as greater imaging depths. Overall, these advantages enable visualization of tumours *in situ* at the cellular level of resolution<sup>8,9</sup>. Condeelis and co-workers have used this method for the intravital imaging of tumour cell behaviour in both orthotopic tumour transplant models and transgenic mice that express GFP<sup>10</sup>. To understand another aspect of angiogenesis, Fukumura *et al.*<sup>24,25</sup> monitored the activity of the vascular endothelial growth factor (VEGF) promoter in transgenic mice that expressed GFP under the control of the VEGF promoter. MPLSM showed that the tumour was able to induce activity of the VEGF promoter and subsequent blood-vessel formation.

Overall, these results show that the interaction of tumour cells with their vascular environment is complex. Tumour cells also seem to be highly motile and can significantly alter their shape to squeeze down narrow vessels. They can also form micrometastases inside larger vessels as well as becoming intimately associated with the vessel wall. These visual findings are intriguing and indicate that we still have much to learn about the tumour–endothelial cell interaction process.

**Imaging metastatic cells.** The metastatic process is complex and depends largely on the composition of the tumour microenvironment, the characteristics of the primary tumour and the ‘soil’ of the distant organ that influences growth of the metastatic ‘seed’. In addition, the initial method used to introduce cancer cells into an animal model can affect the metastatic processes. Imaging these processes in intact animal models and tissues should enable us to learn more about the tumour microenvironment and its effects on metastasis.

Imaging tumours in bone is an important feature of intravital GFP imaging, as it is a clinically prominent site for metastasis. A GFP-expressing MDA-MB-435 human **breast carcinoma** cell line produces widespread osteolytic skeletal metastases following injection into the left ventricle of the heart<sup>26</sup>. Osseous metastases localized predominantly to TRABECULAR BONE regions, especially the proximal and distal femur, the proximal tibia, the proximal humerus and the lumbar vertebrae — locations that are consistent with bone metastatic patterns seen in human breast cancer patients. GFP expression also permitted *ex vivo* detection of single cells and microscopic metastases in bone at early time points.

Rat tongue carcinoma cell lines expressing GFP have been used to investigate the formation of micrometastases. The cells were injected into the portal vein and tracked using intravital video microscopy<sup>27</sup>. The two cell types — LM–GFP metastatic and E2–GFP

non-metastatic tongue carcinoma cells — got stuck in the sinusoidal vessels near the TERMINAL PORTAL VENULES. The E2–GFP cells disappeared from the liver sinusoid within 3 days, whereas a substantial number of LM–GFP cells remained in the liver — possibly because these cells formed stable attachments to the sinusoidal wall. On examination with a CONFOCAL LASER-SCANNING MICROSCOPE, only LM–GFP cells were found to have grown in the liver. Since then, others have demonstrated how sites of cell growth might depend on the site where the cells were initially injected. For example, Mook *et al.*<sup>28</sup> noted that the initial arrest of CC531S–GFP rat-colon cancer cells in sinusoids of the liver was because of a size restriction. Moreover, Sturm *et al.*<sup>29</sup> injected GFP-expressing murine colon carcinoma cells into the spleen of immunocompetent BALB/c mice. Some of these tumour cells were trapped in the PRESINUSOIDAL VASCULATURE as well as in the sinusoids. In addition, some of the tumour cells became attached to the vessel wall and others were also seen to extravasate. Metastases were established in the liver in this mouse model.

Wong and colleagues<sup>30</sup> showed that the death in the lungs of transformed, metastatic GFP-expressing rat embryo cells occurred by apoptosis 24 to 48 hours after injection into the circulation. The researchers established that **BCL2** overexpression conferred resistance to apoptosis *in vivo* for 24 to 48 hours following injection, leading to a greater number of macroscopic metastases being established. These findings add weight to the argument that suppressing apoptosis might enhance the metastatic capacity of tumour cells.

In another study of lung metastasis, Condeelis *et al.*<sup>10</sup> used GFP-expressing metastatic (MTLn3) and non-metastatic (MTC) cell lines (derived from the rat mammary adenocarcinoma 13762 NF cell line) to measure tumour cell density in the blood and to identify individual tumour cells and metastases in the lungs. Metastatic cells showed a greater affinity for blood vessels whereas the non-metastatic cells lost part of their cytoplasm when interacting with the vessel wall. This might be a result of the shearing of cell pseudopods that are inserted into the blood flow during intravasation<sup>10</sup>. These results demonstrate that an important difference between metastatic and non-metastatic cells is their ability to intravasate, a difference that is evident in the primary tumour. It is not known why the metastatic cells are not damaged by the blood flow.

These examples show that these techniques enable the visualization of the steps of metastasis at the cellular level and provide a fresh insight into the complexities of this process *in vivo*.

**Colour-coding metastatic cells.** It is thought that metastases are clonal and originate from rare cells in primary tumours, which are genotypically and phenotypically heterogeneous. Studies using DNA microarray analyses challenge this hypothesis and indicate that the genetic background of the host is an important determinant of metastatic potential, implying that metastases are not necessarily clonal.

**MULTIPHOTON LASER-SCANNING MICROSCOPY**  
Multiphoton laser scanning microscopy (MPLSM) enables the production of long time-lapse recordings from live fluorescent specimens because it uses small beams of infrared light to illuminate only a small area of tissue at a time. So, in living tissue, damage is minimized and, because the light beam penetrates deeply, a greater volume of tissue can be examined.

**TRABECULAR BONE**  
Non-cortical spongy-bone-containing lacunae. Trabecular bone contains the bone marrow.

**TERMINAL PORTAL VENULES**  
Tributaries of the portal vein.

**CONFOCAL LASER-SCANNING MICROSCOPE**  
A microscope designed to minimize out-of-focus contributions from the vertical axis to an image. A pinhole aperture eliminates out-of-focus contributions.

**PRESINUSOIDAL VASCULATURE**  
Branches of the portal vein that leave the sinusoid.

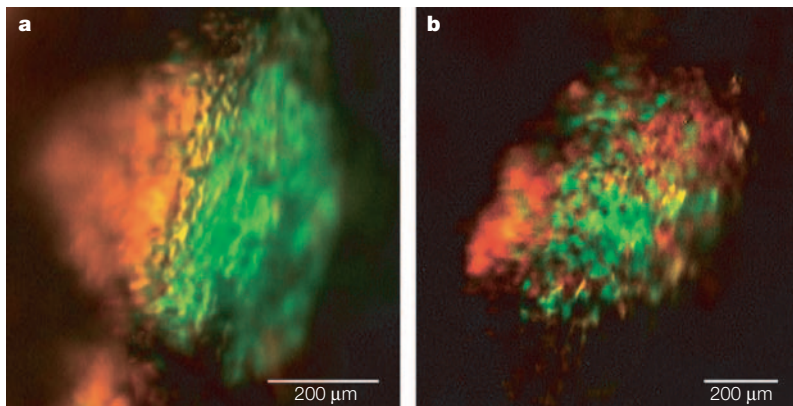


**Figure 2 | Are metastases clonal?** After mixed implantation in severe combined immunodeficient mice green fluorescent protein (GFP)-labelled or red fluorescent protein (RFP)-labelled HT-1080 human fibrosarcoma cells were used to determine the clonality of metastatic colonies. **a** | Two clonal lung colonies, one GFP-expressing, the other RFP-expressing, growing next to one another. **b** | A non-clonal mixed red and green fluorescent RFP-GFP colony. Reproduced with permission from REF. 31 © (2003) American Association for Cancer Research.

Previous methods of determining the clonality of metastases used complicated karyotype or molecular analyses, thereby limiting the number of metastatic colonies analyzed and the conclusions that could be drawn. Yamamoto *et al.*<sup>31</sup> described the use of GFP-labelled or RFP-labelled HT-1080 human fibrosarcoma cells to determine clonality by simple fluorescence visualization of metastatic colonies after mixed implantation into SEVERE COMBINED IMMUNODEFICIENT (SCID) MICE. The resulting pure red or pure green colonies were scored as clonal, whereas mixed red and green colonies were scored as non-clonal (FIG. 2). Analysis of the resulting lung colonies showed that 95% were either pure green or pure red, indicating clonal origin, whereas 5% were composed of red and green cells, indicating non-clonal origin. The clonality of the lung metastases was found to be dependent on the number of cells injected.

Glinskii *et al.*<sup>32</sup> reported that GFP-expressing orthotopic human prostate carcinomas efficiently delivered viable metastatic cells to the host circulation. This is in contrast to the ectopic tumours of the same lineage, which do not deliver live cells into the circulation. Co-implantation of an equivalent mixture of GFP-expressing human prostate tumour cells, previously isolated from the circulation, and parental RFP-expressing human prostate carcinoma cells into the prostate has shown that the GFP-labelled, previously circulating cells are more metastatic than the RFP-labelled parental cells. Berezovskaya *et al.*<sup>33</sup> subsequently demonstrated that the metastatic human prostate carcinoma cells selected for survival in the circulation have increased resistance to ANOIKIS because of increased expression of the X-linked inhibitor of apoptosis protein (XIAP).

These techniques enable the visualization and distinction of tumour cell types that have different properties in the live animal. The colour-coding techniques can also be applied to visualizing the action of specific genes on tumour growth and metastasis.

The inter- $\alpha$ -trypsin inhibitor (ITI) family — a group of proteins built up from different combinations of one light chain (ITIL) and three homologous heavy chains (ITIH1, ITIH2 and ITIH3) — might have a role in metastasis. GFP imaging helped determine which chain of the molecule could inhibit metastasis and/or primary tumour growth. Paris *et al.*<sup>34</sup> constructed human H460M lung cancer cell lines that expressed both GFP and only one of the chains. These clones were subcutaneously injected into NUDE MICE and lung metastasis number and primary tumour weight were determined by GFP expression after 28 days. Expression of the ITIL chain decreased the primary tumour weight and extent of lung metastasis. However, expression of the ITIH1 and ITIH3 chains reduced metastasis, but did not decrease the primary tumour weight.

Nucleoside diphosphate kinase A (NDPKA), encoded by the *NM23H1* gene, functions as a metastasis suppressor in certain human tumours, including breast tumours. However, evidence also points to NDPKA functioning as a metastasis promoter in other human tumours, including neuroblastoma. To test whether NDPKA promotes neuroblastoma metastasis, Almgren *et al.*<sup>35</sup> established stable transfectants and an orthotopic xenograft animal model using the human neuroblastoma cell-line NB69. GFP expression in these cells established that overexpressed NDPKA or the mutant NDPKA(S120G) increased both the number and size of lung metastases without significantly affecting primary tumour development. Compared with the wild-type protein, NDPKA(S120G) seems more effective in promoting metastasis, and provides the first evidence that NDPKA is a metastasis promoter in human neuroblastoma.

By colour-coding different subpopulations of cancer cells it is possible to investigate the metastatic capacity of different cancer cells and also to understand how the expression of particular proteins drives or inhibits metastasis. However, unlike other metastasis models *in vivo*, GFP-expressing cells enable examination of these processes at the cellular level, allowing direct visualization of how and why non-metastatic cells die. This also enables the harvesting of metastatic cells from the blood to examine the genetic changes that have occurred in these surviving cells.

**Imaging dormant tumour cells.** In some instances, viable tumour cells are seen by fluorescent protein expression to lodge in the lung but not grow, a process termed dormancy that might be organ specific. Fluorescent protein imaging enables us to visualize whether a cell that reaches a distant organ will proliferate, arrest or die and to establish the factors that influence this process.

Large detectable metastases did not form after nude mice were given an intravenous injection of chromosome-6-transduced tumour cells expressing GFP<sup>36</sup>. However, fluorescence microscopy showed micrometastases (single cells or clusters of fewer than 10 cells) in the lungs, indicating that these cells were present but had failed to proliferate. When isolated

#### SEVERE COMBINED IMMUNODEFICIENT (SCID) MICE

Mice that are homozygous for the SCID mutation have compromised B-cell and T-cell immunity. This lack of immunity means that they can support human tumour xenografts for preclinical studies.

#### ANOIKIS

Apoptosis resulting from a lack of cellular adhesion.

#### NUDE MICE

Strains of athymic mice bearing the recessive allele *nu/nu* that are mostly hairless and lack all, or most, of the T-cell population. Nude mice can accept either allografts or xenografts. *nu/nu* alleles on some backgrounds have near-normal numbers of T-cells.

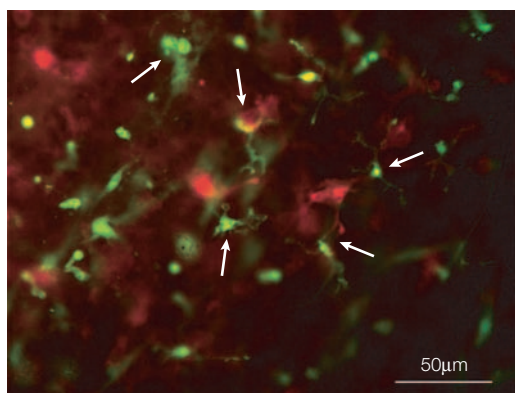


**Figure 3 | Dual-colour tumour–host interactions.** The image shows dendritic-cell-like, green fluorescent protein (GFP)-expressing host cells directly contacting B16F10–red fluorescent protein (RFP)-expressing melanoma cells (interactions between cells indicated by arrows). This image was taken from a GFP-expressing transgenic mouse injected with RFP-expressing tumour cells. Reproduced with permission from REF. 39 © (2003) National Academy of Sciences of the USA.

from the lungs up to 60 days after the injection, these cells were able to grow in culture and formed tumours when injected into the skin; therefore, the cells were still viable but were dormant in the lung. This result implies that some genes on chromosome 6 interfere specifically with growth in the lung but not in the skin.

An ISOGENIC pair of metastatic (M4A4) and non-metastatic (NM2C5), GFP-labelled human breast cancer cell lines derived from the same patient and inoculated into the mammary glands of nude mice were used to investigate the dissemination patterns and fate of cells that escaped spontaneously from the resulting tumours. After tumours appeared, single fluorescent tumour cells were regularly seen in the lungs, even in animals inoculated with NM2C5, which fail to form secondary tumours in other organs. The sensitivity of the technique confirmed the continuing presence of scattered NM2C5 cells in the lung after primary tumour resection, although they formed no metastases by 6 months. These self-disseminated human tumour cells were retrievable from the tissues and were still viable and malignant, manifested by indefinite proliferation *in vitro* and local tumorigenicity *in vivo*. Therefore, these scattered tumour cells were rendered indefinitely quiescent by the microenvironment of the lung tissue<sup>37</sup>.

The capacity to see dormant tumour cells *in vivo* should enhance our understanding of dormant cells and might help us address why cancer patients can relapse many years after the eradication of the primary tumour. This is especially true for breast cancer patients.

**Imageable tumour–host models.** Tumour development is significantly influenced by the surrounding stromal cells. GFP imaging has enabled, for the first time, the visualization of tumour-associated stromal cells and their interaction with tumour cells in the living state. A transgenic GFP mouse with ubiquitous

GFP expression has been developed — the  $\beta$ -actin promoter drives GFP expression in essentially all tissues<sup>38</sup>. In adult mice, these tissues include the heart, lungs, spleen, pancreas, oesophagus, stomach and duodenum. RFP-expressing human cancer cell lines, including PC-3–RFP prostate cancer, HCT-116–RFP colon cancer, MDA-MB-435–RFP breast cancer and HT1080–RFP fibrosarcoma, were transplanted into transgenic GFP nude mice<sup>39</sup>. All of these human tumours grew extensively and showed the details of the tumour–stroma interaction. The GFP-expressing tumour vasculature, both nascent and mature, of the host transgenic GFP mouse could be readily distinguished and seen to interact with the RFP-expressing tumour cells. Interactions between the host immune system and the transplanted tumours could also be seen. GFP-positive, antigen-expressing dendritic cells were observed in contact with RFP-expressing tumour cells through their dendrites (FIG. 3). GFP-expressing macrophages were also observed engulfing RFP-expressing cancer cells. In an immunocompetent transgenic GFP mouse, GFP lymphocytes were seen surrounding cells of an RFP mouse breast tumour, which eventually regressed<sup>39</sup>.

The origin of the tumour stroma is thought to be the normal host tissue. An unanswered question is whether these host cells also become tumorigenic. One hypothesis is that the normal cells fuse with the tumour cells and become tumorigenic. If this is the case, then in the GFP host–RFP tumour model such fused cells should be yellow, showing the usefulness of fluorescent proteins in addressing these important questions. Duda *et al.*<sup>40</sup> noted at the time of transplantation that tumour fragments contain ‘passenger’ cells — endothelial cells and other stromal cells from the original host. They investigated the fate of GFP-labelled endothelial and non-endothelial stromal cells after transplantation into syngeneic (genetically identical) mice. Angiogenic stroma associated with tumour tissue or adipose tissue persisted when transplanted, remained functional and governed the initial neovascularization of grafted tissue fragments for more than 4 weeks after implantation. The passenger endothelial cells survived longer than other stromal cells, which were replaced by host-activated fibroblasts after 3 weeks. The transplantability of tumour stroma indicates that the angiogenic potential of a tumour xenograft depends on the presence of passenger endothelial cells and other stromal cells within the xenograft.

These examples show how informative the visualization of the interaction between tumour and host cells in the live animal, in real time, can be.

#### **Whole-body imaging with fluorescent proteins**

**Advantages.** The fluorescent approach has several important advantages over other optical approaches to imaging tumour growth *in vivo*. Expression of firefly luciferase can be used to visualize tumour growth and regression in response to various therapies in mice. However, the luciferase reporter technique requires that animals are anaesthetized and restrained so

ISOGENIC  
Having the same genetic background, such as two cell lines that might differ only in a gene of interest.

that sufficient photons can be collected to construct a pseudo-image. Furthermore, this process must be carried out in an almost light-free environment and animals must be injected with the luciferin substrate, which has to reach every tumour cell to be useful. Detection of *Luc*-labelled cells *in vivo* is limited to 3,000 human tumour cells<sup>41,42</sup> and the clearance of the luciferin results in an unstable signal<sup>43</sup>. These limitations preclude studies that would be perturbed by anaesthesia, restraint or substrate injection and also makes high-throughput screening infeasible.

In comparison with the luciferase reporter, GFP has a much stronger signal and can therefore be used to image unrestrained animals — irradiation with non-damaging blue light is the only step needed. Real images can be captured using fairly simple apparatus and there is no need for total darkness. The fluorescence intensity of GFP is very strong<sup>44–48</sup> and the protein sequence of GFP has also been ‘humanized’, which enables efficient expression in mammalian cells<sup>49</sup>. In addition, GFP fluorescence is largely unaffected by the external environment as the chromophore is protected by the three-dimensional structure of the protein<sup>50</sup>.

A lentiviral vector expressing a triple fusion vector that harbours a *Renilla* luciferase reporter gene, a reporter gene encoding a monomeric RFP, and a mutant herpes simplex virus (HSV)-type thymidine kinase positron emission tomography reporter, enabled a direct comparison of these imaging techniques *in vivo*. A sensitive, cooled, charge-coupled device camera, compatible with both luciferase and fluorescence imaging, was used to compare the luciferase and fluorescent signals from nude mice bearing 293T cells that expressed the lentiviral vector. The RFP-signal was approximately 1,000 times stronger than that of the luciferase reporter<sup>51</sup>. Because of these advantages, we expect GFP models to supersede the luciferase models.

**Applications.** Being able to visualize tumours growing in animals without the need for any form of invasive surgery has huge benefits for medical science, particularly as it will enable the full process of tumorigenesis, treatment, regression and metastasis, or recurrence, to be seen in one animal. The first use of GFP for whole-body imaging was by Yang *et al.*<sup>1,52</sup> They showed that GFP-expressing primary and metastatic tumour growth could be visualized in numerous organs using whole-body imaging<sup>1</sup>.

Expression of an exogenous GFP protein in specific tissues in intact animals can also be visualized using whole-body imaging. Organs in both nude and normal mice were labelled by injecting the tissues with an adenovirus expressing GFP. Five to eight hours after adenoviral–GFP injection, the fluorescence of the expressed GFP in brain and liver, for example, became visible, and whole-body images were recorded at time-lapse video rates. The GFP fluorescence continued to increase for at least 12 hours following injection and remained detectable in the liver for up to 4 months. This method

requires only that a gene of interest or promoter be fused or operatively linked to GFP<sup>52</sup>.

Whole-body optical imaging of tumour angiogenesis was demonstrated by injecting GFP-expressing Lewis lung carcinoma cells into a subcutaneous site in the footpad of nude mice. In GFP-expressing tumours, the non-luminous induced capillaries were clearly visible against the tumour fluorescence. The footpad is relatively transparent, with few resident blood vessels, allowing quantitative imaging of tumour angiogenesis in the intact animal. Capillary density increased at a constant rate over 10 days, as determined by whole-body imaging. Similarly, GFP-expressing human breast tumour cells, MDA-MB-435, were orthotopically transplanted to the mouse fat pad, where whole-body optical imaging showed that blood vessel density also increased at a constant rate over a 20-week period. The GFP-expressing angiogenesis mouse models can be used for real-time *in vivo* evaluation of agents that inhibit or promote tumour angiogenesis in physiological microenvironments<sup>53</sup>.

In another study, an RFP-expressing human pancreatic tumour cell line was introduced as tissue fragments into the pancreas by surgical implantation into nude mice<sup>54</sup>. The tumour area was measured using RFP imaging and was found to correlate with the tumour volume measured in the opened animal. This validates the use of whole-body imaging to quantify tumour growth and metastasis (FIG. 4). Furthermore, whole-body imaging with this model was used to compare standard and experimental agents for the treatment of pancreatic cancer<sup>55</sup>.

Peyruchaud and colleagues<sup>56</sup> established a GFP-expressing bone-metastasis subclone of MDA-MB-231 breast cancer cells (B02/GFP.2) that grows preferentially in bone. Whole-body fluorescence imaging of the live mice showed that bone metastases could be detected about a week before radiologically distinctive osteolytic lesions developed. Furthermore, when the tumour-bearing mice were treated with a bisphosphonate, the progression of established osteolytic lesions and the expansion of the breast cancer cells in the bone were inhibited. Using whole-body GFP imaging, Peyruchaud *et al.*<sup>57</sup> also showed that the angiogenesis inhibitor angiostatin inhibited tumour growth in bone by inhibiting osteoclast activity.

In another study, however, GFP-expressing tumours could not be detected using whole-body imaging until 7 days after subcutaneous tumour cell inoculation<sup>58</sup>. These results contrast with the results described above. This discrepancy shows the need to use appropriate instrumentation and techniques for whole-body imaging to avoid problems with adequate lighting, contrast and magnification conditions.

These results demonstrate that whole-body imaging using GFP can allow cancer growth, progression and metastasis to be visualized in real time, even at the cellular level. This new technology can be used to understand cancer as a continuing process and to rapidly screen for new drugs.

### Imaging the efficacy of therapeutics

The properties of fluorescent proteins that enable whole-body imaging in real time also mean that the efficacy of therapeutic anticancer treatments can be seen directly without the need for any invasive

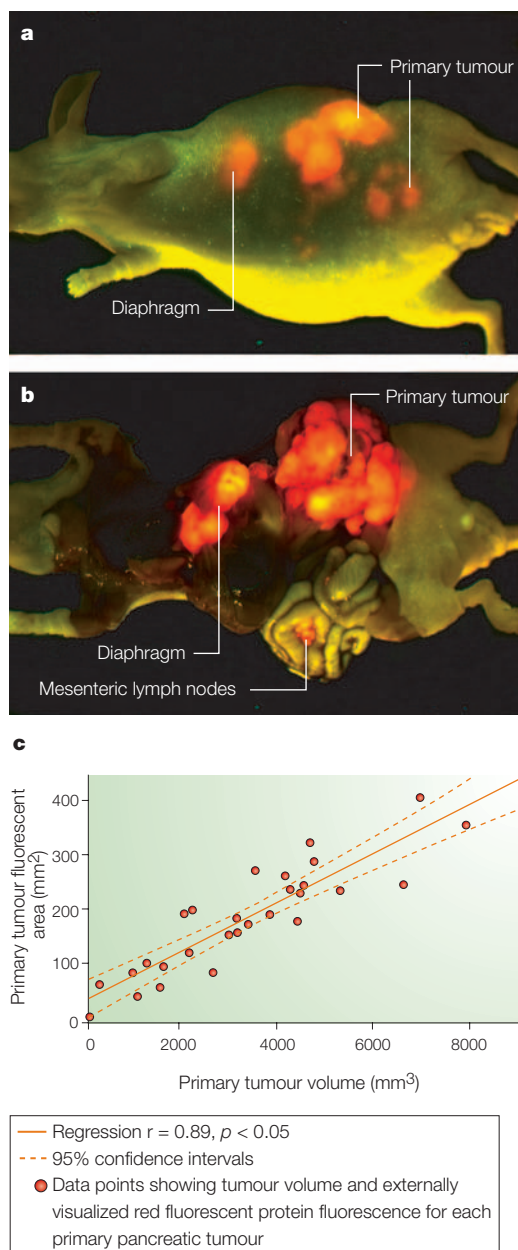


**Figure 4 | A comparison of external and internal quantitative imaging.** The images show extensive locoregional and metastatic growth of red fluorescent protein-expressing Mia-PaCa-2 human pancreatic cancer cells. The images show either the whole-body image (a) or the image gathered after autopsy (b). The tumour load, as determined by whole-body imaging, significantly correlates with traditional measurements obtained after autopsy as shown in the graph (c;  $r = 0.89$ ). The presence of abdominal ascites only slightly reduces the accuracy of such measurements ( $r = 0.83$ ) when compared with mice without ascites ( $r = 0.95$ ). Reproduced with permission from REF. 54 © (2003) Elsevier Science.

procedure in the tumour-bearing mouse. In effect, each animal serves as its own control when whole-body imaging is used to follow drug efficacy — a radical departure from sacrificing mice at each time point and comparing the results. Examples include the use of GFP- or RFP-expressing orthotopic metastatic models treated with candidate antimetastatic agents<sup>55</sup> (FIG. 5). In addition, the response to surgical-resection followed by adjuvant treatment has been assessed by whole-body imaging of GFP- or RFP-expressing tumours<sup>5</sup>.

Such techniques can also be used to analyse the effect of specific anticancer treatments on known genetic backgrounds. Fluorescent protein imaging, especially whole-body imaging, enables rapid analysis of the effects of single or multiple gene changes on cancer aggressiveness and drug sensitivity. Using a mouse model harbouring primary, genetically modified MYC-driven lymphomas that express GFP, whole-body imaging showed that disruption of apoptosis downstream of p53 by BCL2 confers a highly aggressive tumour phenotype, which metastasizes throughout the mouse body<sup>59</sup> (FIG. 6). Moreover, whole-body imaging shows that MYC-driven GFP-expressing lymphomas with p53 or INK4A and ARF mutations, or that overexpress BCL2, respond poorly to cyclophosphamide therapy *in vivo* compared with wild-type cells<sup>60</sup>.

These real-time fluorescent imaging techniques will increase our ability to discover new drugs and genes that mitigate cancer growth and progression. Moreover, such techniques should also enable scientists to clearly see at what stage tumours become resistant to specific treatments and might highlight other ways to circumvent drug resistance.

### Can fluorescent proteins be used in humans?

Although it is possible to express fluorescent proteins in mouse models of human tumours using retroviral or liposomal delivery of the gene, many of these gene-expression techniques are not at the stage where their use, other than in preclinical trials, is ethically approved. However, in principle, the idea of labelling a primary tumour in a patient and then following that tumour throughout the treatment regimen would revolutionize cancer treatment. One use for fluorescent proteins in humans would be to label the tumour before treatment and then monitor for fluorescence after treatment to identify possible recurrence or metastases. In a proof-of-principle experiment, Hasegawa *et al.*<sup>61</sup> showed that injection of a GFP-expressing retroviral vector into a nude mouse resulted in expression of GFP specifically in human stomach cancer cells growing in the peritoneum. Over time, widespread GFP expression, representing the growth and metastasis of the tumour, became evident. No normal tissues were found to be transduced by the GFP-expressing retrovirus. Therefore, reporter-gene transduction of the primary tumour enabled detection of its subsequent metastases. Future human studies could use intra-operative transfection with highly efficient vectors encoding fluorescent proteins that would enable visualization of tumour recurrence after

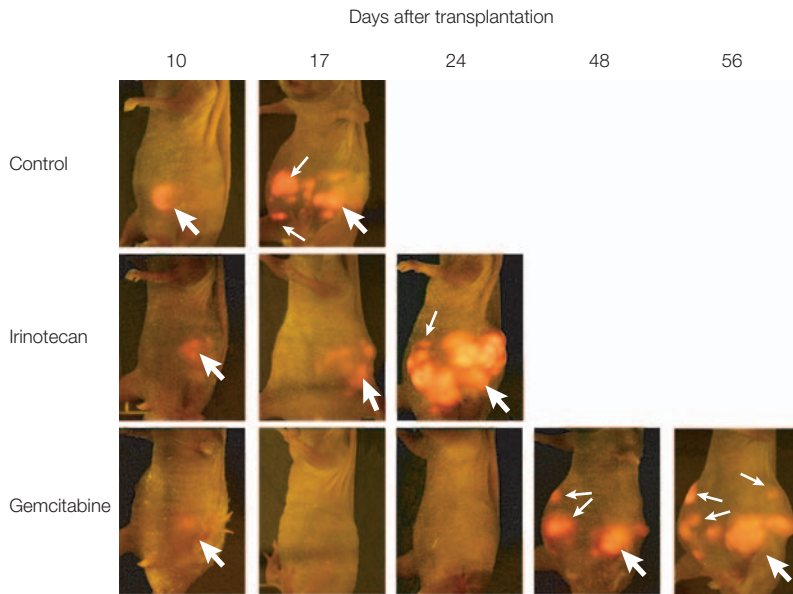


**Figure 5 | Whole-body imaging to monitor tumour cell growth and treatment efficacy.** This series of images show Mia-PaCa-2 pancreatic cancer (expressing red fluorescent protein) progression and evaluation of therapeutic efficacy over time. The images were obtained using real-time whole-body imaging of representative mice from each treatment group on days 10, 17, 24, 48 and 56 after tumour implantation. Thick arrows show the primary tumour and thin arrows indicate metastases. Treatment with irinotecan suppressed primary and metastatic tumour growth compared with controls. Gemcitabine successfully induced temporary regression of disease over the first month, after which growth and distant metastasis of the tumour accelerated despite continued treatment. Reproduced with permission from REF. 54 © (2003) Elsevier Science.

surgery by the use of fluorescence endoscopy and other optical methods. Tumour cells that integrate a copy or copies of the GFP-expressing retroviral vector into their DNA will ensure that GFP remains expressed by the progeny of the tumour cells. This, in theory, would mean that tumour cells that survived chemotherapy or radiotherapy would be detectable once they started to proliferate after treatment. Alternatively, gene therapy techniques could be linked to a GFP label.

To ensure tumour-specific expression, GFP linked to a tumour-specific promoter could be introduced systemically, and only the tumour cells would express the GFP plasmid. To determine whether the carcino-embryonic antigen (CEA) promoter could control expression of the *GFP* gene, human MKN45-GFP stomach cancer cells were injected into the peritoneal cavity of BALB/c nude mice<sup>62</sup>. A CEA-E GFP (E denotes brighter fluorescence) plasmid was then introduced into the peritoneal cavity using liposomes. GFP-fluorescent tumour nodules were subsequently detected by FLUORESCENCE STEREOIMCROSCOPY. In another approach, GFP was conjugated to the transferrin promoter to target disseminated human erythroleukaemia cells (K562) *in vivo*<sup>63</sup>. When *GFP*-gene conjugates were systemically administered, through the tail vein, to nude mice that had been subcutaneously inoculated with tumour cells, GFP expression was only detected in the target cells.

Varda-Bloom and colleagues<sup>64</sup> developed a tissue-specific adenoviral vector with a view to developing a

gene-based therapy that would inhibit angiogenesis in tumour metastases. They expressed GFP under the murine preproendothelin 1 (*Edn1*) promoter that is activated in endothelial cells during angiogenesis. High levels of expression and specific activity of EDN1 were seen after the systemic administration of the adenoviral vector to mice bearing Lewis lung carcinoma metastases. GFP expression was detected in the new vasculature of the primary tumours and also in the lung metastases, with the highest expression evident in the angiogenic endothelial cells of the metastases.

Umeoka *et al.*<sup>65</sup> described a new approach for visualizing tumours by using a tumour-specific replication-competent adenovirus in combination with Ad-GFP, a replication-deficient adenovirus expressing GFP. An adenovirus 5 vector (OBP-301) was constructed in which the human telomerase reverse transcriptase (*TERT*) promoter element (which is active in the tumour cells) drives expression of the adenovirus immediate-early genes *E1A* and *E1B* (necessary for adenoviral replication), linked to an INTERNAL RIBOSOME ENTRY SITE. When human lung cancer and colon cancer cell lines were infected with replication deficient Ad-GFP at a low multiplicity of infection, GFP expression could not be detected. In the presence of OBP-301, however, Ad-GFP replicated and showed strong green fluorescence in the tumour cells. By contrast, co-infection with OBP-301 and Ad-GFP did not show any fluorescence in normal cells such as fibroblasts and vascular endothelial cells because of the low levels of activity of the telomerase promoter. Subcutaneous tumours in nude mice injected with OBP-301 and Ad-GFP became fluorescent within 3 days of administration of the virus. Moreover, intrathoracic administration of Ad-GFP and OBP-301 labelled disseminated intrathoracic A549 lung tumour nodules in mice.

However, not all expression studies have been successful to date. GFP expressed from a herpes simplex virus-1/Epstein-Barr virus vector has been administered to tumour-bearing animals and persistent GFP expression was not achieved<sup>66</sup>. Subsequent analyses indicated that expression from the vector was blocked by DNA methylation or other processes.

Although much future work is required, all these results indicate that fluorescent proteins might eventually be clinically useful in cancer patients.

**Conclusions and future directions**

Tumour cells stably expressing GFP and other fluorescent proteins *in vivo* are a powerful new tool for cancer research. Stability of expression has been studied by Naumov *et al.*<sup>8</sup> who noted that all the Chinese hamster ovary (CHO)-K1-GFP cells used in their study were stably fluorescent (measured by flow cytometry) even after 24 days of growing in medium in the absence of vector-selective antibiotics. This finding implies that GFP can be stably expressed in cells *in vivo*. This feature has proved true for all cells studied so far and is exemplified by the generation of extensive GFP-expressing metastases.

**FLUORESCENCE STEREOIMCROSCOPY**

A microscope with two oculars that is equipped with a light source and filters for excitation of a fluorescence molecule and for the visualization of the resulting emission light.

**INTERNAL RIBOSOME ENTRY SITE**

A region of DNA that codes for a messenger RNA sequence that can bind to ribosomes, which is often used to genetically link two proteins that would still be translated separately but be controlled by one promoter.

## NEAR-INFRARED

The near-infrared region of the electromagnetic spectrum (covering a wavelength range of 700 nm to 3  $\mu$ m) lies just beyond the sensitivity of the human eye.

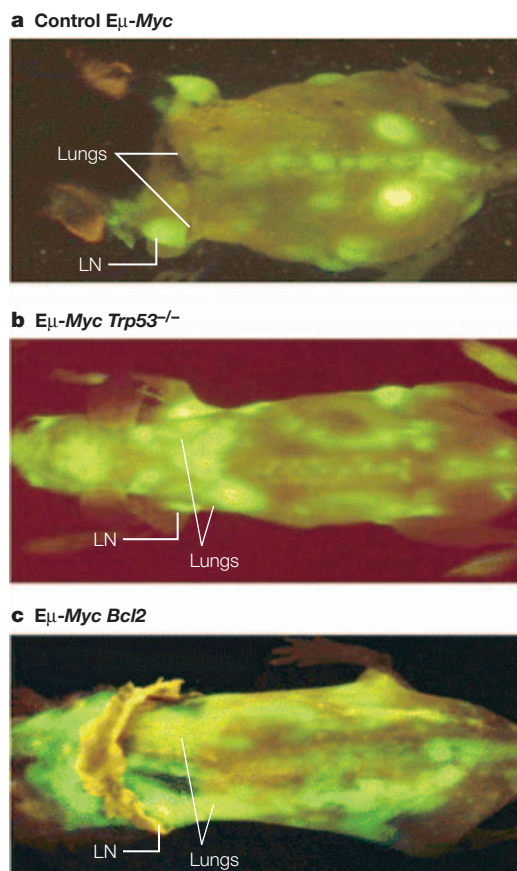


**Figure 6 | Whole-body fluorescence imaging of lymphoma progression in live mice.** The images show the temporal and spatial progression of E $\mu$ -Myc lymphoma cells, tagged with green fluorescent protein, which were transplanted into mice. These cells were either control (a) or expressed either a mutant p53 protein (b) or the anti-apoptotic protein BCL2 (c). Each image is taken from a live mouse using whole-body imaging. The E $\mu$ -Myc lymphomas expand within the lymphoid compartments and bone, whereas the mutant p53 and the BCL2-overexpressing lymphomas readily disseminate into non-lymphoid compartments. Reproduced with permission from REF. 59 © (2002) Elsevier Science. LN, lymph node.

The use of GFP-expressing tumour cells in fresh tissue or live animals<sup>1,2,4,6,8,10,11,15,40,67</sup> has provided new insights into the real-time growth and metastatic behaviour of cancer. Several independent studies, which include an extensive comparison between

metastases of GFP-transduced carcinoma and the parental cell lines<sup>9,29,68</sup>, have shown that GFP or RFP transduction and expression does not affect metastatic behaviour<sup>29</sup>.

Further developments look set to expand the use of *in vivo* GFP imaging. An improved method of whole-body GFP imaging has made use of a laser excitation source and band-pass filters matched specifically to GFP and constitutive tissue fluorescence emission bands. Processing of the primary GFP fluorescence images acquired by the charge-coupled device camera can now be subtracted from background tissue autofluorescence. This approach achieved 100% sensitivity and specificity for *in vivo* detection of the 10% of GFP expressing cells within a population of BxPc3-GFP pancreatic tumour cells that were grafted subcutaneously or implanted orthotopically into the pancreases of nude mice<sup>69</sup>.

NEAR-INFRARED probes that can be activated by proteases<sup>70-72</sup> can also be used for optical imaging of tumours. This approach requires that the tumour expresses a specific protease that cleaves the injected probe so that it becomes fluorescent. However, tumours in tissues such as the liver, where normal cells express many different active proteases, cannot be visualized because the background signals are too high.

The applications of *in vivo* cellular imaging with fluorescent proteins should expand with the development of proteins with new colours. Shaner *et al.*<sup>73</sup> have taken the RFP from *Discosoma* and converted it through multiple amino-acid substitutions into a monomer. With further genetic modification this group have created a series of modified proteins with new colours from yellow-orange to red-orange. These new coloured proteins include mBanana, tdTomato, mTangerine and mStrawberry, with increasingly longer emission maxima. It is expected that many additional coloured proteins will be isolated from various organisms and modified to produce even more colours. The availability of many different coloured proteins will enable simultaneous imaging of multiple cellular events *in vivo*, surpassing what can currently be visualized both *in vivo* and *in vitro*. Fluorescent protein imaging is enabling not only whole-body imaging but, because of its cellular resolution and multiple colours, it is giving rise to a new field of *in vivo* cell biology.

- Yang, M. *et al.* Whole-body optical imaging of green fluorescent protein-expressing tumors and metastases. *Proc. Natl Acad. Sci. USA* **97**, 1206–1211 (2000).  
**The first paper to demonstrate whole-body imaging using GFP-expressing tumours.**
- Yang, M. *et al.* Direct external imaging of nascent cancer, tumor progression, angiogenesis, and metastasis on internal organs in the fluorescent orthotopic model. *Proc. Natl Acad. Sci. USA* **99**, 3824–3829 (2002).
- Yamamoto, N. *et al.* Real-time imaging of individual color-coded metastatic colonies *in vivo*. *Clin. Exp. Metastasis* **20**, 633–638 (2003).
- Brown, E. B. *et al.* *In vivo* measurement of gene expression, angiogenesis and physiological function in tumors using multiphoton laser scanning microscopy. *Nature Med.* **7**, 864–868 (2001).
- Katz, M. H. *et al.* Survival efficacy of adjuvant cytosine-analogue CS-682 in a fluorescent orthotopic model of human pancreatic cancer. *Cancer Res.* **64**, 1828–1833 (2004).
- Chishima, T. *et al.* Cancer invasion and micrometastasis visualized in live tissue by green fluorescent protein expression. *Cancer Res.* **57**, 2042–2047 (1997).  
**The first paper to use GFP to visualize cancer cells in vivo.**
- Jain, R. K., Munn, L. L. & Fukumura, D. Dissecting tumour pathophysiology using intravital microscopy. *Nature Rev. Cancer* **2**, 266–276 (2002).
- Naumov, G. N. *et al.* Cellular expression of green fluorescent protein, coupled with high-resolution *in vivo* videomicroscopy, to monitor steps in tumor metastasis. *J. Cell Sci.* **112**, 1835–1842 (1999).
- Farina, K. L. *et al.* Cell motility of tumor cells visualized in living intact primary tumors using green fluorescent protein. *Cancer Res.* **58**, 2528–2532 (1998).
- Condeelis, J. & Segall, J. E. Intravital imaging of cell movement in tumours. *Nature Rev. Cancer* **3**, 921–930 (2003).
- Chishima, T. *et al.* Metastatic patterns of lung cancer visualized live and in process by green fluorescent protein expression. *Clin. Exp. Metastasis* **15**, 547–552 (1997).
- Huang, M. S. *et al.* Establishment of fluorescent lung carcinoma metastasis model and its real-time microscopic

detection in SCID mice. *Clin. Exp. Metastasis* **19**, 359–368 (2002).

13. Li, C. Y. *et al.* Initial stages of tumor cell-induced angiogenesis: evaluation via skin window chambers in rodent models. *J. Natl Cancer Inst.* **92**, 143–147 (2000).

14. Moore, A., Marecos, E., Simonova, M., Weissleder, R. & Bogdanov, A. Jr. Novel gliosarcoma cell line expressing green fluorescent protein: a model for quantitative assessment of angiogenesis. *Microvasc. Res.* **56**, 145–153 (1998).

15. Al-Mehdi, A. B. *et al.* Intravascular origin of metastasis from the proliferation of endothelium-attached tumor cells: a new model for metastasis. *Nature Med.* **6**, 100–102 (2000).

16. Wong, C. W. *et al.* Intravascular location of breast cancer cells after spontaneous metastasis to the lung. *Am. J. Pathol.* **161**, 749–753 (2002).

17. Yamamoto, N. *et al.* Cellular dynamics visualized in live cells *in vitro* and *in vivo* by differential dual-color nuclear-cytoplasmic fluorescent-protein expression. *Cancer Res.* **64**, 4251–4256 (2004).

**First paper to use dual-colour cancer cells with GFP in the nucleus and RFP in the cytoplasm to visualize nuclear and cellular dynamics in vivo.**

18. Yamauchi, K. *et al.* Real-time *in vivo* dual-color imaging of intracapillary cancer cell and nucleus deformation and migration. *Cancer Res.* **65**, 4246–4252 (2005)

19. Chang, Y. S. *et al.* Mosaic blood vessels in tumors: frequency of cancer cells in contact with flowing blood. *Proc. Natl Acad. Sci. USA* **97**, 14608–14613 (2000).

20. Li, L. *et al.* Nestin expression in hair follicle sheath progenitor cells. *Proc. Natl Acad. Sci. USA* **100**, 9958–9961 (2003).

21. Amoh, Y. *et al.* Nascent blood vessels in the skin arise from nestin-expressing hair follicle cells. *Proc. Natl Acad. Sci. USA* **101**, 13291–13295 (2004).

22. Amoh, Y. *et al.* Hair follicle-derived blood vessels vascularize tumors in skin and are inhibited by doxorubicin. *Cancer Res.* **65**, 2337–2343 (2005).

23. Denk, W., Strickler, J. H. & Webb, W. W. Two-photon laser scanning fluorescence microscopy. *Science* **248**, 73–76 (1990).

24. Fukumura, D., Yuan, F., Monsky, W. L., Chen, Y. & Jain, R. K. Effect of host microenvironment on the microcirculation of human colon adenocarcinoma. *Am. J. Pathol.* **151**, 679–688 (1997).

25. Fukumura, D. *et al.* Tumor induction of VEGF promoter activity in stromal cells. *Cell* **94**, 715–725 (1998).

26. Harms, J. F. & Welch, D. R. MDA-MB-435 human breast carcinoma metastasis to bone. *Clin. Exp. Metastasis* **20**, 327–334 (2003).

27. Ito, S. *et al.* Real-time observation of micrometastasis formation in the living mouse liver using a green fluorescent protein gene-tagged rat tongue carcinoma cell line. *Int. J. Cancer* **93**, 212–217 (2001).

28. Mook, O. R. *et al.* Visualization of early events in tumor formation of eGFP-transfected rat colon cancer cells in liver. *Hepatology* **38**, 295–304 (2003).

29. Sturm, J. W. *et al.* Enhanced green fluorescent protein-transfection of murine colon carcinoma cells: key for early tumor detection and quantification. *Clin. Exp. Metastasis* **20**, 395–405 (2003).

30. Wong, C. W. *et al.* Apoptosis: an early event in metastatic inefficiency. *Cancer Res.* **61**, 333–338 (2001).

31. Yamamoto, N. *et al.* Determination of clonality of metastasis by cell-specific color-coded fluorescent-protein imaging. *Cancer Res.* **63**, 7785–7790 (2003).

32. Glinskii, A. B. *et al.* Viable circulating metastatic cells produced in orthotopic but not ectopic prostate cancer models. *Cancer Res.* **63**, 4239–4243 (2003).

33. Berezovskaya, O. *et al.* Increased expression of apoptosis inhibitor protein XIAP contributes to anoikis resistance of circulating human prostate cancer metastasis precursor cells. *Cancer Res.* **65**, 2378–2386 (2005).

34. Paris, S. *et al.* Inhibition of tumor growth and metastatic spreading by overexpression of inter- $\alpha$ -trypsin inhibitor family chains. *Int. J. Cancer* **97**, 615–620 (2002).

35. Almgren, M. A., Henriksson, K. C., Fujimoto, J. & Chang, C. L. Nucleoside diphosphate kinase A/nm23-H1 promotes metastasis of NB69-derived human neuroblastoma. *Mol. Cancer Res.* **2**, 387–394 (2004).

36. Goldberg, S. F., Harms, J. F., Quon, K. & Welch, D. R. Metastasis-suppressed C8161 melanoma cells arrest in lung but fail to proliferate. *Clin. Exp. Metastasis* **17**, 601–607 (1999).

37. Goodison, S. *et al.* Prolonged dormancy and site-specific growth potential of cancer cells spontaneously disseminated from non-metastatic breast tumors as revealed by labeling with green fluorescent protein. *Clin. Cancer Res.* **9**, 3808–3814 (2003).

38. Okabe, M., Ikawa, M., Kominami, K., Nakanishi, T. & Nishimune, Y. 'Green mice' as a source of ubiquitous green cells. *FEBS Lett.* **407**, 313–319 (1997).

**First development of a mouse with GFP in essentially all cells.**

39. Yang, M. *et al.* Dual-color fluorescence imaging distinguishes tumor cells from induced host angiogenic vessels and stromal cells. *Proc. Natl Acad. Sci. USA* **100**, 14259–14262 (2003).

**First dual-colour tumour-host model. The model uses RFP-tumours transplanted into GFP mice.**

40. Duda, D. G. *et al.* Differential transplantability of tumor-associated stromal cells. *Cancer Res.* **64**, 5920–5924 (2004).

41. Sweeney, T. J. *et al.* Visualizing the kinetics of tumor-cell clearance in living animals. *Proc. Natl Acad. Sci. USA* **96**, 12044–12049 (1999).

42. Contag, C. H., Jenkins, D., Contag, P. R. & Negrin, R. S. Use of reporter genes for optical measurements of neoplastic disease *in vivo*. *Neoplasia* **2**, 41–52 (2000).

43. Burgos, J. S. *et al.* Time course of bioluminescent signal in orthotopic and heterotopic brain tumors in nude mice. *Biotechniques* **34**, 1184–1188 (2003).

44. Morin, J. & Hastings, J. Energy transfer in a bioluminescent system. *J. Cell. Physiol.* **77**, 313–318 (1971).

45. Cormack, B., Valdivia, R. & Falkow, S. FACS-optimized mutants of the green fluorescent protein (GFP). *Gene* **173**, 33–38 (1996).

46. Cramer, A., Whitehorn, E. A., Tate, E. & Stemmer, W. P. C. Improved green fluorescent protein by molecular evolution using DNA shuffling. *Nature Biotechnol.* **14**, 315–319 (1996).

47. Delagrè, S., Hawtin, R. E., Silva, C. M., Yang, M. M. & Youvan, D. C. Red-shifted excitation mutants of the green fluorescent protein. *Biotechnology* **13**, 151–154 (1995).

48. Heim, R., Cubitt, A. B., Tsien, R. Y. Improved green fluorescence. *Nature* **373**, 663–664 (1995).

**References 47 and 48 were the first papers to generate GFP mutants in the chromophore to increase fluorescence as well as new colours.**

49. Zolotukhin, S., Potter, M., Hauswirth, W. W., Guy, J. & Muzyczka, N. A 'humanized' green fluorescent protein cDNA adapted for high-level expression in mammalian cells. *J. Virol.* **70**, 4646–4654 (1996).

50. Cody, C. W., Prasher, D. C., Welster, W. M., Prendergast, F. G. & Ward, W. W. Chemical structure of the hexapeptide chromophore of the *Aequorea* green fluorescent protein. *Biochemistry* **32**, 1212–1218 (1993).

**First paper to demonstrate the chromophore amino acid sequence in GFP. This paper enabled later studies to generate brighter mutants and new colours.**

51. Ray, P., De, A., Min, J. J., Tsien, R. Y. & Gambhir, S. S. Imaging tri-fusion multimodality reporter gene expression in living subjects. *Cancer Res.* **64**, 1323–1330 (2004).

52. Yang, M., Baranov, E., Moossa, A. R., Penman, S. & Hoffman, R. M. Visualizing gene expression by whole-body fluorescence imaging. *Proc. Natl Acad. Sci. USA* **97**, 12278–12282 (2000).

53. Yang, M. *et al.* Whole-body and intravital optical imaging of angiogenesis in orthotopically implanted tumors. *Proc. Natl Acad. Sci. USA* **98**, 2616–2621 (2001).

54. Katz, M. H. *et al.* A novel red fluorescent protein orthotopic pancreatic cancer model for the preclinical evaluation of chemotherapeutics. *J. Surg. Res.* **113**, 151–160 (2003).

55. Katz, M. H. *et al.* Selective antimetastatic activity of cytosine analog CS-682 in a red fluorescent protein orthotopic model of pancreatic cancer. *Cancer Res.* **63**, 5521–5525 (2003).

56. Peyruchaud, O. *et al.* Early detection of bone metastases in a murine model using fluorescent human breast cancer cells: application to the use of the bisphosphonate zoledronic acid in the treatment of osteolytic lesions. *J. Bone Miner. Res.* **16**, 2027–2034 (2001).

57. Peyruchaud, O., Serre, C.-M., NicAmhlaibh, R., Fournier, P. & Clezardin, P. Angiostatin inhibits bone metastasis formation in nude mice through a direct anti-osteoclastic activity. *J. Biol. Chem.* **278**, 45826–45832 (2003).

58. Choy, G. *et al.* Comparison of noninvasive fluorescent and bioluminescent small animal optical imaging. *Biotechniques* **35**, 1022–1026 and 1028–1030 (2003).

59. Schmitt, C. A. *et al.* Dissecting p53 tumor suppressor functions *in vivo*. *Cancer Cell* **1**, 289–298 (2002).

60. Schmitt, C. A. *et al.* A senescence program controlled by p53 and p16<sup>INK4a</sup> contributes to the outcome of cancer therapy. *Cell* **109**, 335–346 (2002).

61. Hasegawa, S. *et al.* *In vivo* tumor delivery of the green fluorescent protein gene to report future occurrence of metastasis. *Cancer Gene Ther.* **7**, 1336–1340 (2000).

**First paper to transform cancer cells in vivo with GFP. This is a model for future clinical applications of fluorescent proteins.**

62. Kaneko, K. *et al.* Detection of peritoneal micrometastases of gastric carcinoma with green fluorescent protein and carcinoembryonic antigen promoter. *Cancer Res.* **61**, 5570–5574 (2001).

63. Sato, Y. *et al.* *In vivo* gene delivery to tumor cells by transferrin-streptavidin-DNA conjugate. *FASEB J.* **14**, 2108–2118 (2000).

64. Varda-Bloom, N. *et al.* Tissue-specific gene therapy directed to tumor angiogenesis. *Gene Ther.* **8**, 819–827 (2001).

65. Umeoka, T. *et al.* Visualization of intrathoracically disseminated solid tumors in mice with optical imaging by telomerase-specific amplification of a transferred green fluorescent protein gene. *Cancer Res.* **64**, 6259–6265 (2004).

66. Qi, J., Link, C. J., Wang, S. Direct observation of GFP gene expression transduced with HSV-1/EBV amplicon vector in unfixed tumor tissue. *Biotechniques* **28**, 206–208 (2000).

67. Chishima, T. *et al.* Visualization of the metastatic process by green fluorescent protein expression. *Anticancer Res.* **17**, 2377–2384 (1997).

68. Lu, J.-Y. *et al.* Establishment of red fluorescent protein-tagged HeLa tumor metastasis models: determination of DsRed2 insertion effects and comparison of metastatic patterns after subcutaneous, intraperitoneal, or intravenous injection. *Clin. Exp. Metastasis* **20**, 121–133 (2003).

69. Wack, S. *et al.* Feasibility, sensitivity, and reliability of laser-induced fluorescence imaging of green fluorescent protein-expressing tumors *in vivo*. *Mol. Ther.* **7**, 765–773 (2003).

70. Weissleder, R., Tung, C. H., Mahmood, U. & Bogdanov, A. Jr. *In vivo* imaging of tumors with protease-activated near-infrared fluorescent probes. *Nature Biotechnol.* **17**, 375–378 (1999).

71. Bremer, C., Tung, C. H. & Weissleder, R. *In vivo* molecular target assessment of matrix metalloproteinase inhibition. *Nature Med.* **7**, 743–748 (2001).

72. Jiang, T. *et al.* Tumor imaging by means of proteolytic activation of cell-penetrating peptides. *Proc. Natl Acad. Sci. USA* **101**, 17867–17872 (2004).

73. Shaner, N. C. *et al.* Improved monomeric red, orange and yellow fluorescent proteins derived from *Discosoma* sp. red fluorescent protein. *Nature Biotechnol.* **22**, 1567–1572 (2004).

74. Verkhusha, V. & Lukyanov, K. A. The molecular properties and applications of Anthozoa fluorescent proteins and chromoproteins. *Nature Biotechnol.* **22**, 289–296 (2004).

**Review of new fluorescent proteins from the group that cloned the first RFP.**

75. Zimmer, M. Green fluorescent protein (GFP): applications, structure and related photophysical behavior. *Chem. Rev.* **102**, 759–781 (2002).

76. Yang, M., Luiken, G., Baranov, E. & Hoffman, R. M. Facile whole-body imaging of internal fluorescent tumors in mice with an LED flashlight. *Biotechniques* **39**, 170–172 (2005).

77. Levenson, R., Yang, M. & Hoffman, R. M. Whole-body dual-color differential fluorescence imaging of tumor angiogenesis enhanced by spectral unmixing. *Proc. Am. Assoc. Cancer Res.* **45**, 46 (2004).

Competing interests statement  
The author declares competing financial interests: see web version for details

 Online links

**DATABASES**  
The following terms in this article are linked online to Entrez Gene: <http://www.ncbi.nlm.nih.gov/entrez/query.fcgi?db=gene> BCL2 | CD105 | CD31 | MYC | NDPKA | nestin | p53  
**National Cancer Institute:** <http://www.cancer.gov>  
breast carcinoma | neuroblastoma  
**FURTHER INFORMATION**  
Robert Hoffman's homepage: [www.anticancer.com](http://www.anticancer.com)  
Access to this interactive links box is free online.